

Investigation of the Tsujun Bridge damage mechanism during the 2016 Kumamoto earthquake

Aiko FURUKAWA¹, Hiroki YOSHIKAWA¹ and Junji KIYONO¹

Investigation of the Tsujun Bridge damage mechanism during the 2016 Kumamoto earthquake

Aiko FURUKAWA¹, Hiroki YOSHIKAWA¹ and Junji KIYONO¹

Abstract

Tsujun Bridge, a stone arch bridge, suffered slight damage during the 2016 Kumamoto earthquake. In this study, a microtremor observation was conducted, the natural frequencies of the bridge were estimated, and the horizontal-to-vertical (H/V) spectral ratios at Tsujun Bridge and at a strong-motion observation site were calculated. The ground motion for Tsujun Bridge was estimated based on H/V spectral ratios, and a numerical model was created based on the observed natural frequencies. The seismic response of the numerical model was simulated using the refined distinct-element method, and the damage mechanism during the Kumamoto earthquake was investigated.

Key words : Tsujun Bridge; stone arch bridge; damage mechanism; 2016 Kumamoto earthquake; microtremor observation; refined distinct-element method

1. Introduction

Tsujun Bridge is a stone arch bridge located in Yamato Town, Kumamoto Prefecture, Japan (Fig. 1(a)). This is a stone aqueduct bridge whose construction was completed in 1854, and which has since been designated as an important cultural property of Japan. The water pipe consists of stones with a hole, as shown in Fig. 1(b). Fig. 1(c) shows a sectional view of the top of the bridge in

the transverse direction. There are wall stones on both sides and three stone pipes inside. The spaces between the stone pipes and those between the wall stones and the stone pipes are filled with soil (Yamato Town of Kumamoto Prefecture, 2015).

During the foreshock and mainshock of the Kumamoto earthquake on April 14 and 16 in 2016, Tsujun Bridge suffered slight damage. Although stones did not fall, various wall stones were pushed

¹ Department of Urban Management, Graduate School of Engineering, Kyoto University, Kyoto City, Japan

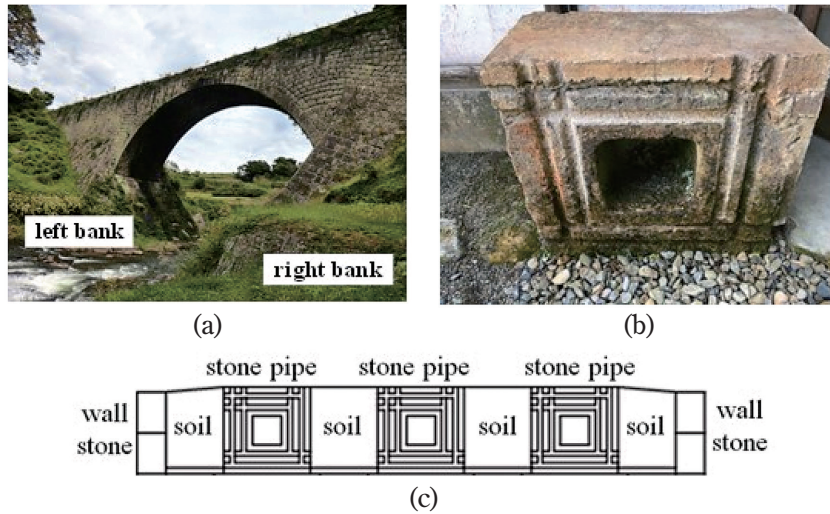


Fig. 1 Tsujun bridge: (a) appearance from the upstream side; (b) stone pipe; (c) section view of the top of the bridge in the transverse direction (revised based on Yamato Town of Kumamoto Prefecture (2015)).

out in the transverse direction and cracks occurred inside the soil filling the spaces between the wall stones and the stone pipes, as shown in Fig. 2(a) (Yamato Town of Kumamoto Prefecture, 2016a). Fig. 2(b) shows a contour of movement displacement for the wall stones in the transverse direction during a series of Kumamoto earthquake vibrations (Yamato Town of Kumamoto Prefecture, 2016b). The displacement was calculated from the results of a three-dimensional survey conducted before the earthquake in 2013 and after the earthquake in 2016. The red color indicates the maximum displacement. The displacement was small at the arch crown but larger between the arch support and the bridge deck edge. A maximum displacement of approximately 15 cm was observed on the right-bank side of the upstream side. In Fig. 2(c), the red line indicates the location of the cracks observed inside the soil (Yamato Town of Kumamoto Prefecture, 2016c). Cracks in the soil were found between the arch support and the bridge deck edge, but not at the arch crown. Cracks in the soil were observed in the exterior soil between the wall stones and the

stone pipes. The crack length has been reported to be approximately 1 to 2 cm (Yamato Town of Kumamoto Prefecture, 2016c).

Research regarding the damage to Tsujun Bridge is still insufficient. Izuno et al. (2017) conducted microtremor observation on and around Tsujun Bridge to estimate the natural frequencies. They also conducted simplified penetration testing and estimated the stiffness of the supporting ground. They modeled the bridge with a single-degree-of-freedom system based on the observed natural frequencies, and conducted seismic response analysis. They input the ground motion record observed at the nearest strong-motion observation site (K-NET YABE) (NIED: National Research Institute for Earth Science and Disaster Resilience), which is 0.9 km from Tsujun Bridge. Hagiwara et al. (2017) conducted seismic response analysis for Tsujun Bridge using the three-dimensional finite-element method. They modeled the bridge with linear elements using the abovementioned observed ground motion data as input. However, they modeled only the bridge and not the side ground.

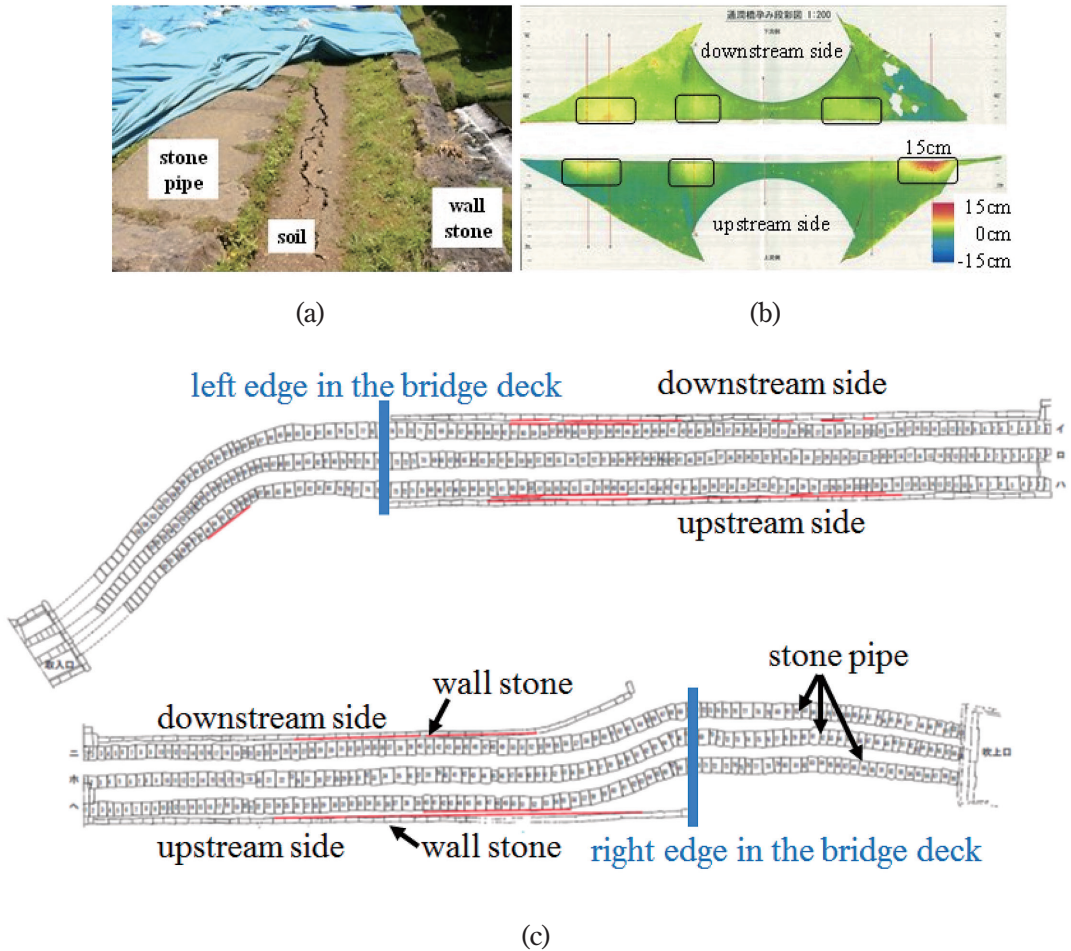


Fig. 2 Damage to Tsujun Bridge caused by the Kumamoto earthquake: (a) movement of wall stones and cracks in the soil (Yamato Town of Kumamoto Prefecture, 2016a); (b) contour of wall stone displacement in the transverse direction (Yamato Town of Kumamoto Prefecture, 2016b); (c) locations of crack occurrence in the soil (red color) (revised based on Yamato Town of Kumamoto Prefecture (2016c)).

In their results, the maximum displacement and maximum stress occurred at the arch crown, which is different from the actual damage. As mentioned previously, the actual displacement of the wall stones and the actual cracks in the soil were observed not at the arch crown but rather between the arch support and the bridge deck edge. In this regard, the damage mechanism of Tsujun Bridge has not yet been clarified.

Given this background, the objective of this

study is to clarify the damage mechanism of Tsujun Bridge during the Kumamoto earthquake. We used the refined distinct-element method (refined DEM), which is suitable for three-dimensional elastic, failure, and collapse behaviors (Furukawa et al., 2011). We conducted microtremor observation on the bridge and on the side ground surface, and estimated their natural frequencies. The numerical model was developed such that the analytical natural frequencies of the bridge and side ground

matched the observed values. We also conducted microtremor observation on the base ground surface of Tsujun Bridge and at the strong-motion observation site (K-NET YABE) to estimate the horizontal-to-vertical (H/V) spectral ratios. Because the H/V spectral ratios at the two sites have different characteristics, intuition suggests that the ground motion at Tsujun Bridge is different from that of K-NET YABE. Therefore, we estimated the ground motion for Tsujun Bridge during the Kumamoto earthquake.

According to the literature (Yabe Town of Kumamoto Prefecture, 1984), the basement of Tsujun Bridge seems to be attached to the bedrock. Therefore, we computed the bedrock ground motion at K-NET YABE based on multiple-reflection theory, and assumed it to be the input ground motion for Tsujun Bridge. We termed this ground motion “estimated ground motion 1.” Additionally, we employed an empirical method to correct the observed ground motion using the H/V spectral ratios at the two sites (Nakamura et al., 2009). We termed the ground motion estimated using this empirical method “estimated ground motion 2.” Then, the seismic responses of Tsujun Bridge and the side ground during the Kumamoto earthquake were simulated. We investigated the mechanism

of the actual damage that occurred between the arch support and the bridge deck edge from the viewpoint of frequency characteristics. Moreover, we investigated the severity of ground motion required for the wall stones to fall and collapse of the arch system to occur.

2. Microtremor observation

2.1 Overview

To investigate the vibration characteristics, we conducted microtremor observation at Tsujun Bridge and at the strong-motion observation site. At the bridge, microtremors were observed at the arch crown (point 1), at the mid-point between the arch crown and the bridge deck edge on the right-bank side (point 2), on the side ground surface on the right-bank side (point 3), on the base ground surface on the right-bank side (point 4), and on the base ground surface on the left-bank side (point 5). Moreover, microtremors were observed at K-NET YABE, which is the strong-motion observation site operated by NIED. K-NET YABE is 0.9 km from Tsujun Bridge. The observation point locations are shown in Fig. 3. The first microtremor observation was conducted at points 1, 2, and 5 and at K-NET YABE on October 4, 2016. Considering that the modeling of side grounds is important, a second

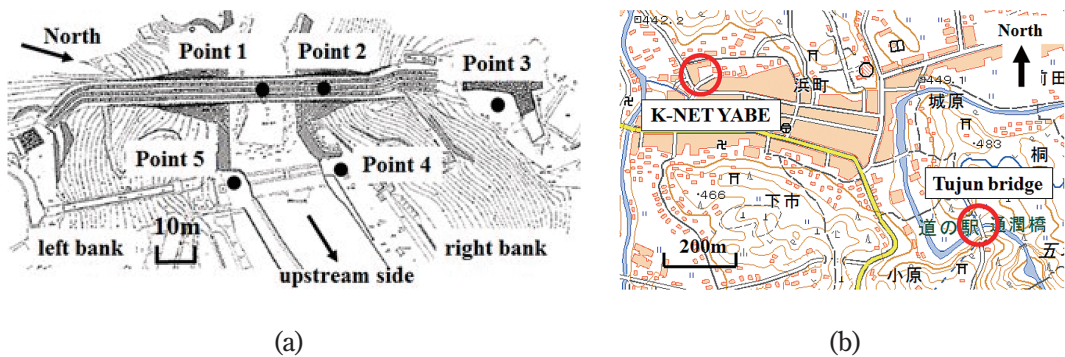


Fig. 3 Microtremor observation points: (a) measurement locations at Tsujun Bridge (Yamato Town of Kumamoto Prefecture, 2015); (b) location of Tsujun Bridge and K-NET YABE (Geospatial Information Authority of Japan).

microtremor observation was conducted at points 3 and 4 on November 1, 2017.

The measurement was conducted for 12 minutes at each point. The sampling interval for the measurement data was 0.01 s. The measured waveforms were corrected with regard to the baseline and divided into segments of 4,096 data points. Thus, their mean Fourier amplitudes were computed. For smoothing, a Parzen window with a frequency bandwidth of 0.4 Hz was applied.

2.2 Natural frequencies and damping ratios of Tsujun Bridge

Fig. 4 shows the Fourier spectra for the accelerations observed at the bridge at points 1 and 2 in three directions. Since the transfer functions at points 1 and 2 with regard to the base ground (point 4 or 5) were not observed, we estimate the first-mode natural frequencies and damping ratios in three directions using the acceleration Fourier spectra at points 1 and 2 assuming that the input force is white noise.

From the figures, the natural frequencies of the first mode were estimated as 4.2 Hz for the longitudinal direction, 2.4 Hz for the transverse direction, and 5.4 Hz for the vertical direction. It is possible that peak frequencies other than first-mode natural frequencies are higher-mode natural frequencies, but it is difficult to determine the modal order

since mode shapes are difficult to draw with two accelerometers. The damping ratios of the first mode were estimated using the half-power method assuming that the input force is white noise. The damping ratios of the first mode were determined as 0.029 for the longitudinal direction, 0.038 for the transverse direction, and 0.030 for the vertical direction.

The peak Fourier amplitudes were observed not at the first-mode natural frequencies, but rather at 11 Hz in the longitudinal direction and at 10 Hz in the transverse direction, because the predominant frequency of the base ground was approximately 10-11 Hz, as will be explained later.

2.3 Natural frequencies of the Tsujun Bridge side ground

Fig. 5 shows the transfer function of the Tsujun Bridge side ground on the right-bank side, which is obtained by taking the ratio of the Fourier spectra on the ground surface side (point 3) to that on the base ground surface (point 4). The natural frequencies of the side ground were estimated as 6.3 Hz in the east-west direction and 6.0 Hz in the north-south direction. Therefore, it was concluded that the natural frequency of the first mode in the horizontal direction was approximately 6.0 Hz. The first-mode natural frequency of the side ground was found to be higher than that of the bridge.

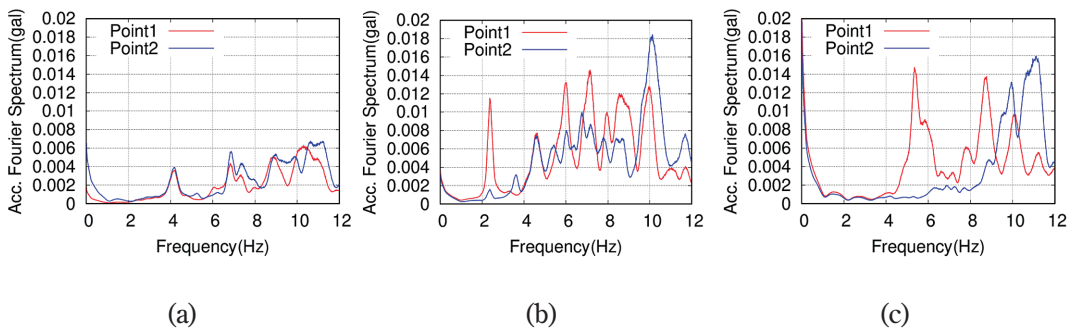


Fig. 4 Fourier spectra of microtremor observation records: (a) longitudinal direction; (b) transverse direction; (c) vertical direction

2.4 H/V spectral ratios at Tsujun Bridge and K-NET YABE

Fig. 6 shows the H/V spectra ratios observed on the base ground surface at Tsujun Bridge (points 4 and 5) and at K-NET YABE. The peak frequencies at Tsujun Bridge were approximately 10-11 Hz, even though there was little difference between the right- and left-bank sides. On the other hand, the peak frequency at K-NET YABE was determined as 7.2 Hz. The amplitude of the H/V spectra at Tsujun Bridge was smaller at 3-9 Hz and larger at 10-11 Hz in comparison with that at K-NET YABE. From these comparisons, it can be considered that the base ground vibration characteristics at the two sites were different even though the two sites were very close with a straight distance of 0.9 km. Therefore, intuition suggests that the ground motion at Tsujun Bridge has characteristics that are different from those observed at K-NET YABE.

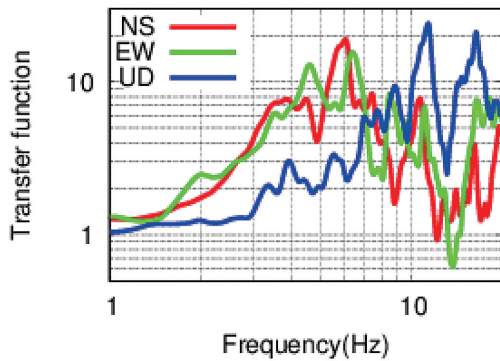


Fig. 5 Transfer function of the side ground on right-bank side.

The microtremor observation results are summarized in Table 1.

3. Estimation of input ground motion for Tsujun Bridge

3.1 Overview

By using microtremor observation, we found that the H/V spectral ratios at Tsujun Bridge and K-NET YABE had different characteristics, and that the ground motion at the two sites was also different. Therefore, this study estimated the ground motion for Tsujun Bridge using two methods. The first method was to input the bedrock ground motion at K-NET YABE as an input to Tsujun Bridge (estimated ground motion 1). The second method is empirical and was used to correct the ground motion at K-NET YABE using the H/V spectral ratios.

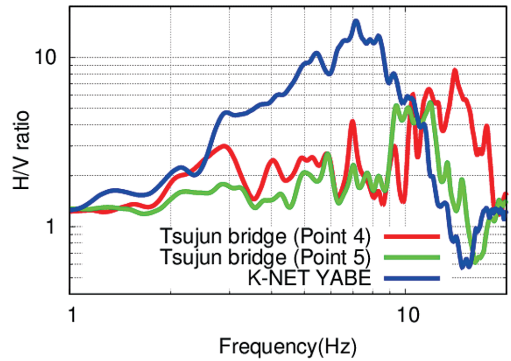


Fig. 6 H/V spectral ratios on the base ground surface at Tsujun Bridge and K-NET YABE.

Table 1 Summary of microtremor observation results.

Location	Tsujun bridge			Side ground of Tsujun Bridge	Base ground of Tsujun Bridge	Base ground of K-NET YABE
	Bridge	Transverse	Vertical	Horizontal	Horizontal	Horizontal
Natural frequency	4.2 Hz	2.4 Hz	5.4 Hz	6.0 Hz	10-11 Hz	7.2 Hz
Damping ratio	0.029	0.038	0.030	—	—	—

3.2 Method 1: Bedrock ground motion at K-NET YABE (estimated ground motion 1)

From the literature (Yabe Town of Kumamoto Prefecture, 1984), the Tsujun Bridge basement seems to be attached to the bedrock. Therefore, we computed the bedrock ground motion at K-NET YABE based on multiple-reflection theory, and considered it as the input ground motion for Tsujun Bridge. We termed this ground motion “estimated ground motion 1.”

The soil profile of the surface ground at K-NET YABE is presented in Table 2 (NIED). We assumed that the height of the bedrock surface was 5 m. The natural frequency of the first mode of the SH wave was calculated as 7.2 Hz, which is in good agreement with that obtained from the H/V spectral ratio. The material was assumed to be linear and the damping ratios for the surface soil were assumed to be 0.05.

3.3 Method 2: Empirical method proposed by Nakamura et al. (estimated ground motion 2)

The second method is empirical and has been proposed by Nakamura et al. (2009). This method corrects the observed ground motion using the H/V spectral ratios at two sites. We termed the ground motion estimated using this empirical method “estimated ground motion 2.”

In this method, modification factors β_O and β_E are defined as follows:

$$\beta_O = \frac{1/C_{Omax}(H/V)_O^M}{(H/V)_O^E}, \beta_E = \frac{1/C_{Emax}(H/V)_E^M}{(H/V)_E^E}. \quad (1)$$

Table 2 Soil profile of the surface ground at K-NET YABE (NIED).

Depth	Density (ton/m ³)	Shear wave velocity (m/s)	Soil type
0-3 m	1.63	90	Clay
4-5 m	2.00	230	Gravel
5 m	2.16	810	Rock

Here, subscripts *O* and *E* indicate the observation point and estimation point, respectively; superscripts *M* and *E* indicate the microtremors and earthquake, respectively; and C_{Omax} and C_{Emax} are the maximum amplitudes of the microtremor H/V spectral ratios at the observation and estimation points, respectively. In summary, modification factors β_O and β_E were obtained by dividing the normalized microtremor H/V spectral ratios by the H/V spectral ratios of the earthquake ground motion.

By introducing modification factors β_O and β_E , the microtremor H/V spectral ratio at the observation and estimation sites can be obtained as follows.

$$\frac{(H/V)_E^M}{(H/V)_O^M} = \frac{C_{Emax}\beta_E(H/V)_E^E}{C_{Omax}\beta_O(H/V)_O^E}. \quad (2)$$

From the above equation, the horizontal Fourier earthquake amplitudes at estimation site H_E^E were obtained using the earthquake’s horizontal Fourier amplitudes at observation site H_O^E and modification factor α , as follows:

$$H_E^E = \alpha \frac{(H/V)_E^M}{(H/V)_O^M} H_O^E. \quad (3)$$

Modification factor α can be estimated as follows:

$$\alpha = \frac{\beta_O}{\beta_E} \cdot \gamma_{E/O} \cdot \frac{1/C_{Emax}}{1/C_{Omax}}, \gamma_{E/O} = \frac{V_E^E}{V_O^E}. \quad (4)$$

In the above equation, to estimate modification factor α , all parameters except modification factor β_E and the spectral ratio of vertical ground motions $\gamma_{E/O}$ can be computed from the H/V spectral ratios. However, modification factor β_E and the spectral ratios of vertical ground motions $\gamma_{E/O}$ cannot be obtained without the earthquake ground motion records at the estimation site. Nakamura et al. (2009) proposed empirical equations to estimate these unknown parameters.

First, we explain how to estimate modification

factor β_E . Nakamura et al. (2009) reported that there is a positive correlation between average β_O and average β_E between the period from 0.1 s to 2 s at nearby stations. They proposed to obtain average β_O of the observation site from 0.1 s to 2 s, and use it as modification factor β_E for the estimation site.

Next, we explain how to estimate the spectral ratio of vertical ground motion $\gamma_{E/O}$. Nakamura et al. (2009) proposed the following estimation equations:

$$Y_{E/O}^I = \left(\frac{1 - C'_{max}}{2} \right) \left(\frac{e^{[T/T_g - 1]} - e^{-[T/T_g - 1]}}{e^{[T/T_g - 1]} + e^{-[T/T_g - 1]}} \right) + \left(\frac{1 + C'_{max}}{2} \right), \quad \gamma_{E/O}^{II} = 1 / \gamma_{E/O}^I. \quad (5)$$

Here, $\gamma_{E/O}^I$ is an estimation equation when the predominant frequency of the observation site's H/V spectral ratio is higher than that of the estimation site, and $\gamma_{E/O}^{II}$ is an estimation equation when the observation site's predominant H/V spectral ratio frequency is lower than that of the estimation site. Moreover, $\gamma_{E/O}$ can be estimated for each period T , and T_g is the larger value of the predominant natural H/V spectral ratio periods for the micro-tremors between the observation and estimation sites. The estimation equation for C'_{max} is as follows:

$$\begin{aligned} C'_{max} &= 1.2 \times C_{max} + 1.6, \\ C_{max} &= \text{MAX}(C_{Omax} / C_{Emax}, C_{Emax} / C_{Omax}). \end{aligned} \quad (6)$$

The Fourier amplitudes of the earthquake ground motion for Tsujun Bridge were estimated by Nakamura's method. The Fourier phase cannot be estimated by this method; thus, the Fourier phase of the observed ground motion at K-NET YABE was used for the Tsujun Bridge site. Finally, the vertical ground motion cannot be estimated by this method.

3. 4 Comparison of observed ground motion and estimated ground motion

Fig. 7 indicates the acceleration time history of the observed ground motion at K-NET YABE (observation), estimated ground motion 1 (estimation 1), and estimated ground motion 2 (estimation 2). Because the two methods can be used only for horizontal ground motion, the observed vertical ground motion at K-NET YABE was used with the estimated horizontal ground motion. Fig. 7 shows the ground motion used as input for the numerical analysis conducted in this study. We combined the foreshock at 21:26 on April 14 and the mainshock at 1:25 on April 16 into one continuous ground motion. The time history consisted of 0 gal for 1 s to maintain stability against gravitational force,

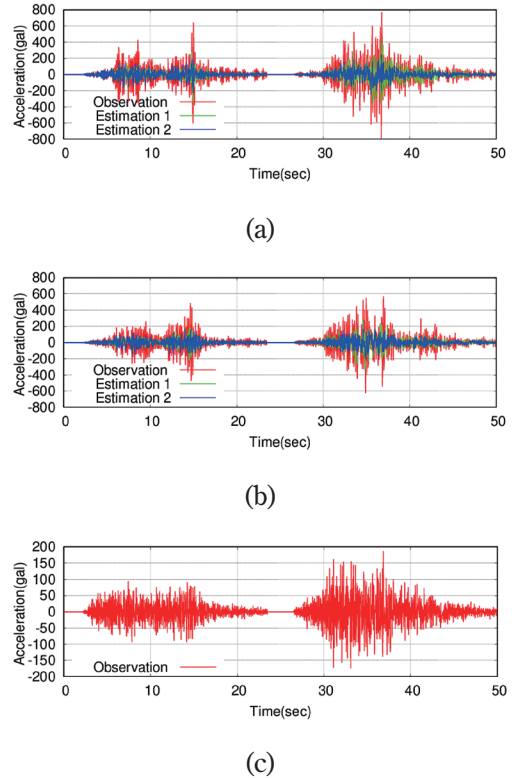


Fig. 7 Acceleration time histories: (a) longitudinal direction; (b) transverse direction; (c) vertical direction.

foreshock for 22.5 s, 0 gal for 1.5 s to dissipate the vibration caused by the foreshock and restore stability, and mainshock for 25 s. The observed motion had the largest peak ground acceleration (PGA), while estimated motion 2 had the smallest PGA.

Fig. 8 shows a comparison of the acceleration Fourier spectra in the horizontal directions. Estimated ground motion 1, which is the bedrock ground motion at K-NET YABE, had a smaller amplitude at approximately 7 Hz, in comparison with

the observed ground motion, because the natural frequency of the K-NET YABE ground surface was 7.2 Hz. Estimated ground motion 2 had a smaller amplitude at approximately 3-9 Hz and a larger amplitude at approximately 10-11 Hz, in comparison with the observed ground motion, owing to the difference in the H/V spectral ratios.

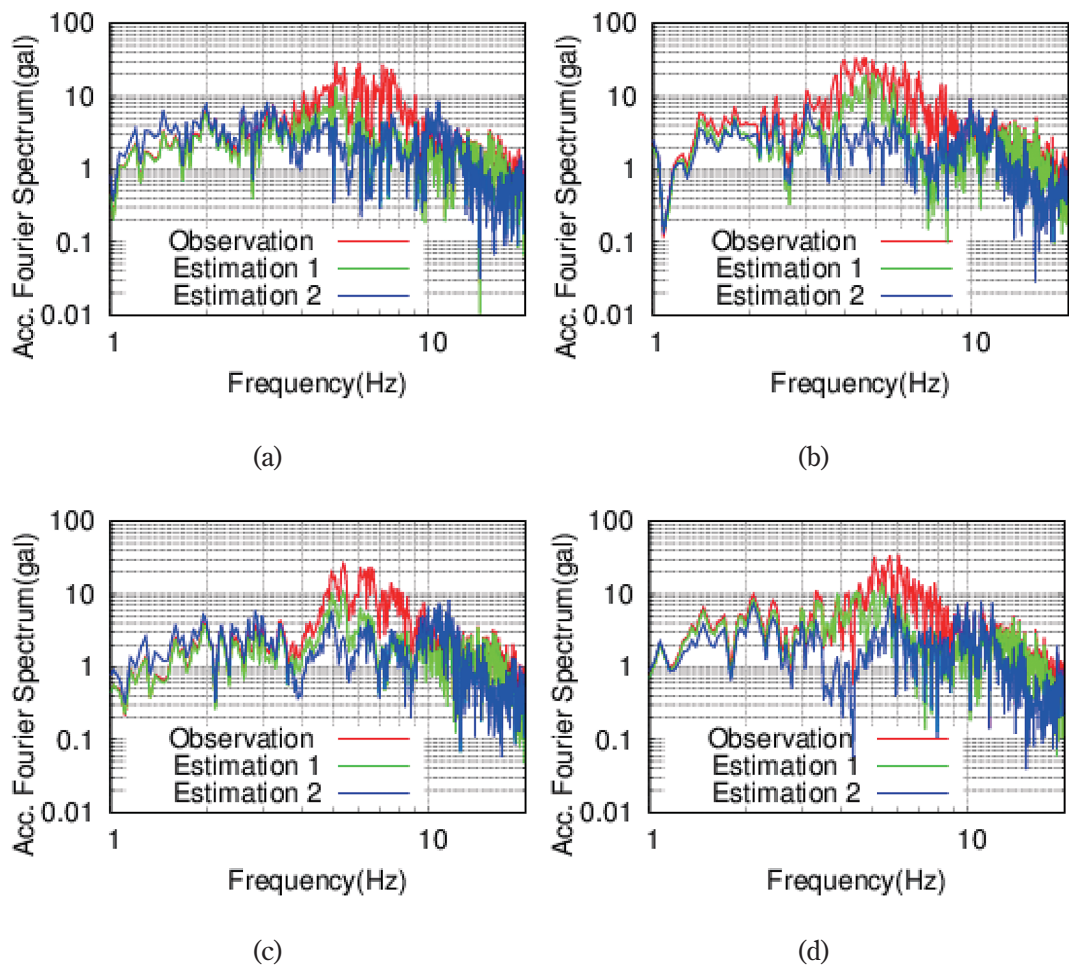


Fig. 8 Fourier acceleration amplitudes: (a) foreshock in the longitudinal direction; (b) mainshock in the longitudinal direction; (c) foreshock in the transverse direction; (d) mainshock in the transverse direction.

4. Development of a numerical model for Tsujun Bridge

4.1 Refined DEM

The refined DEM (Furukawa et al., 2011) is a numerical analysis method that simulates three-dimensional elastic, failure, and collapse behaviors. This method is a refined version of the three-dimensional DEM. The points of difference from the original DEM (Cundall, 1998) are the arrangement of springs, and that the spring constant is theoretically determinable from the material properties.

In the refined DEM, a structure is modeled as an assembly of rigid elements, as in the original DEM. However, unlike the original DEM, the surface of an element is divided into small segments, as shown in Fig. 9(a). The black points indicate the representative point of each segment. One restoring spring and a combination of a contact spring and a dashpot are attached to one segment (Fig. 9(b)) at each of the representative points shown in Fig. 9(a). This segmentation enables the spring constant to be derived theoretically based on the three-dimensional stress-strain relationship of the material and segment area.

Fig. 9(c) shows a spring for computing the restoring force (restoring spring). This spring models the elasticity of the elements. The restoring spring is a set between the continuous elements.

Before failure, the continuous elements are connected by the restoring springs, and the elastic behavior can be simulated. Structural failure is modeled as the breakage of the restoring spring, at which time the restoring spring is replaced with a contact spring and a contact dashpot. Fig. 9(d) shows a spring and a dashpot for computing the contact force (contact spring and dashpot). These model the contact, separation, and recontact between the elements. The dashpots were introduced to represent the energy dissipation caused by the contact. Thus, the interaction between the elements is modeled using multiple springs and multiple dashpots attached to the surface of the elements.

This method enables the simulation of elastic behavior and is suitable for simulating large displacement behaviors such as failure and collapse.

4.2 Numerical model

For the bridge, the area surrounded by the red frame in Fig. 10(a) was modeled. The bridge span was 72.9 m, the width was 6.6 m, and the height was 21.6 m. The entire view of the numerical model and the view of the bridge from above are shown in Fig. 10(b, c). The longitudinal direction and transverse direction are defined as the x- and y-axis, respectively.

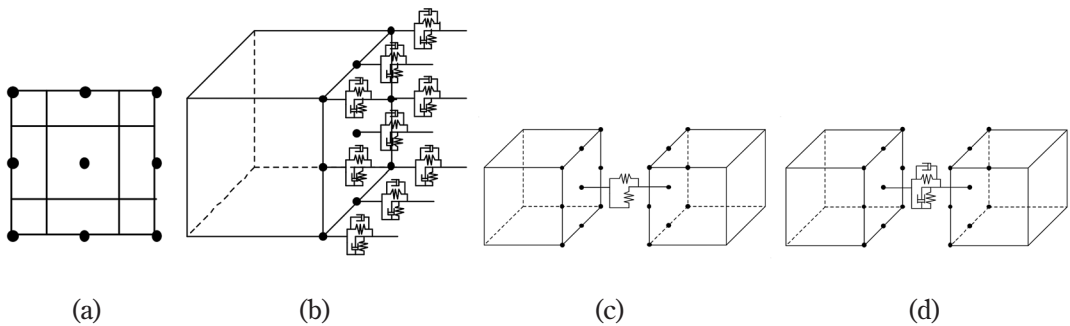


Fig. 9 Model of the spring and dashpot in refined DEM: (a) segments and contact points; (b) multiple springs and multiple dashpots attached to the surface; (c) restoring spring; (d) contact spring and dashpot.

In Fig. 10(b, c, d), all stones except the stone pipes are shown with brown elements. The element size of the stones was approximately 1 m (x) × 1 m (y) × 1 m (z), which is larger than the actual size of approximately 0.6 m (x) × 0.6 m (y) × 0.6 m (z), owing to the limited computational resources. The stone pipe is modeled by a rectangular element with a size of 0.6 m (x) × 0.8 m (y) × 0.8 m (z), as shown for the yellow element in Fig. 10(c). The actual stone pipe has an interior hole of 0.3 m × 0.3

m for water to pass through. Although we used a rectangular element without a hole, we considered the effect of the hole by applying a smaller apparent density.

There is soil between the wall stones and stone pipes, and between the stone pipes, as indicated by the red element in Fig. 10(d). To express the crack, the soil was divided into two elements in the transverse direction.

The surrounding ground is also modeled and indicated by the light gray elements. The ground surrounding the bridge from the upstream and downstream sides is modeled with the same size as the stones. The side grounds of 40 m (x) × 70 m (y) × 21.6 m (z) on both the right- and left-bank sides were also modeled to express the vibration characteristics. The side grounds were divided roughly into elements with a size of 8 m (x) × 7.8 m (y) × 5.4 m (z). The dark gray elements indicate the base ground. From the literature (Yabe Town of Kumamoto Prefecture, 1984), the basement of Tsujun Bridge seems to be attached to the bedrock. Therefore, the dark gray elements were assumed to be fixed.

The total number of elements was 8,204. The surface of each element was divided into nine segments.

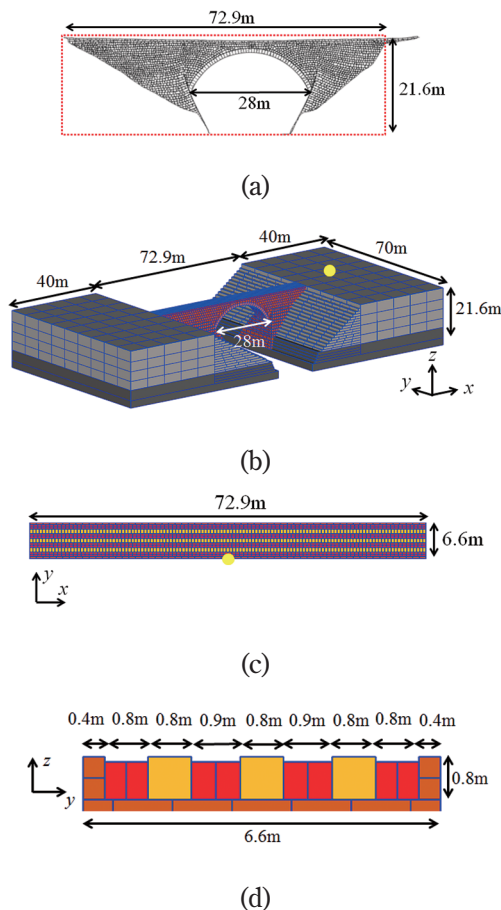


Fig. 10 Numerical model: (a) front view of the bridge and modeled area (Yamato Town of Kumamoto Prefecture, 2015); (b) bird's-eye view of the numerical model; (c) plan view of the Tsujun Bridge model; (d) cross section of the top of the bridge.

4.3 Material properties

The material properties used in the analysis are listed in Table 3.

With regard to the side ground, the shear modulus was determined such that the analytical natural frequency of the first mode matches the natural frequency obtained by microtremor observation. Young's modulus was estimated by assuming that Poisson's ratio is 0.3. We used the same parameters for the ground surrounding the bridge from the upstream and downstream sides. With regard to the bedrock, the same properties as those of the K-NET YABE bedrock were used.

Table 3 Material properties of the numerical model.

	Density (kg/m ³)	Young's modulus (N/m ²)	Poisson's ratio
Stone (not comprising the arch ring)	2.7×10^3	7.2×10^8	0.25
Stone (comprising the arch ring)	2.7×10^3	6.0×10^8	0.25
Stone pipe	2.3×10^3	2.0×10^8	0.25
Soil	1.8×10^3	7.5×10^7	0.30
Surrounding ground	1.8×10^3	1.44×10^9	0.30
Bedrock	2.16×10^3	3.68×10^9	0.30

Table 4 Comparison of natural frequencies between microtremor observation and the numerical model.

Component	Direction	Microtremor Observation (Hz)	Numerical analysis (Hz)	Difference (Hz)
Bridge	Longitudinal direction	4.2	4.7	0.48
Bridge	Transverse direction	2.4	2.3	-0.05
Bridge	Vertical direction	5.4	5.3	-0.09
Side ground	Horizontal	6.0	6.2 (x-direction)	0.16
			5.9 (y-direction)	-0.06

By determining the material properties of the ground in advance, the material properties for the remaining elements, i.e., stone (not comprising the arch ring), stone (comprising the arch ring), stone pipe, and soil, were determined. By referring to the material properties in the literature (NIED; Asai et al., 2009), we set the material properties such that the analytical natural frequencies of the bridge matched the natural frequencies obtained by microtremor observation.

4.4 Verification of the numerical model for linear analysis

The natural frequencies of the first mode for the bridge and the side ground were simulated to verify the developed numerical model and the material properties determined for linear analysis. An acceleration of 100 gal was input for a duration of 0.01 s, and the response was computed as a free vibration in each direction. The strength between the elements was set to be strong enough such that failure could not occur. The acceleration response was computed at the yellow circle point shown in Fig. 10(c) to obtain the free vibration of the bridge, and at the yellow circle point shown in Fig. 10(b)

to obtain the free vibration of the side ground. Table 4 shows the comparison of the first mode's natural frequencies, which were obtained by microtremor observation and numerical analysis.

With regard to Tsujun Bridge, the analytical natural frequencies of the first mode are in good agreement with the observed ones, particularly in the transverse direction and in the vertical direction. Regarding the side ground, the analytical natural frequencies were 6.2 Hz in the x-direction and 5.9 Hz in the y-direction, which were close to the observed natural frequency of 6.0 Hz. From these comparisons, we considered that the numerical model and determined material properties were applicable to a linear analysis of Tsujun Bridge.

4.5 Strength between elements

Next, we determined the strength between the elements to express failure and sliding between the elements. The strength values are listed in Table 5. Since the actual strength is not available, we assumed the strength values in the following manner.

The strength between the stone pipes is the strength of the mortar. The mortar was placed at

Table 5 Strength between elements to model tensile and shear failure.

	Tensile strength (N/m ²)	Bond strength (N/m ²)	Friction coefficient
Stone pipe-Stone pipe (mortar)	1.0×10^5	1.0×10^5	0.584
Stone-Stone/Stone-Stone pipe	1.0×10^2	1.0×10^2	0.669
Stone-Soil/Stone-Ground	1.0×10^2	1.0×10^2	0.584
Soil-Soil/Soil-Ground	1.0×10^2	2.5×10^4	0.372
Ground-Ground	Failure not considered		

the notch shown in Fig. 1(b). The area where the mortar was placed is very small in comparison with the section area of the stone pipe. Because experimental data were not available, we used the strength value recommended as the design specification for masonry (Architectural Institute of Japan, 1964) and modified the value by considering the area where the mortar was placed and the area of the stone pipe element.

With regard to the strength between the stones and the strength between the stone and the stone pipe, the actual strength was equal to zero because there was no mortar in between. However, to obtain numerical stability against gravity, a small value was used for the tensile strength and bond strength.

In the same manner, a small tensile strength was used between the soils and between the soil and the ground. Regarding the bond strength and friction coefficient, the value was determined assuming that the N value of the standard penetration test was approximately equal to 2. Since there are no physical data available for the soil stiffness, we assumed the N value to be 2 based on the findings that the soil settled almost 30 cm by two-step jumps due to the weight during the survey on October 4, 2016.

The friction coefficient was determined by referring to previous research (Asai, 2009).

Thus, a non-linear model was developed for the bridge by considering the failure between the elements. Regarding the non-linearity of the side ground, failure was not considered because failure did not occur during the Kumamoto earthquake.

Conversely, the material non-linearity of the side ground was considered by introducing equivalent linear analysis.

4.6 Non-linearity of the side ground

The non-linearity of the side ground was investigated using equivalent linear analysis. By inputting the material properties of the ground and bedrock (listed in Table 3), equivalent linear analysis was conducted for the three ground motions in the transverse direction (y). The bedrock was assumed to be linear, and the dynamic deformation characteristics proposed by the Public Works Research Institute (PWRI, 1982) were used for the side ground.

The equivalent shear modulus and equivalent damping ratios were obtained, and the equivalent shear modulus was transformed into the equivalent Young's modulus. The results are presented in Table 6. The equivalent Young's modulus became smaller and the equivalent damping ratio became larger as the PGA increased. In the seismic response analysis, the equivalent Young's modulus and damping ratio were used for the ground elements.

4.7 Damping ratio

In the refined DEM, structural damping can be considered as mass-proportional damping. Because the vibration in the transverse direction (y) was dominant, the damping ratio of the bridge components (stone, stone pipe, and soil) was assumed to be 0.038, which is the damping ratio obtained by microtremor observation in the y-di-

Table 6 Equivalent Young's modulus and damping ratio of the ground.

Input ground motion	PGA (y-direction)	Equivalent Young's modulus (N/m ²)	Equivalent damping ratio
Observed motion	626 gal	1.24×10^9	0.053
Estimated motion 1	346 gal	1.25×10^9	0.043
Estimated motion 2	207 gal	1.33×10^9	0.039

rection. For the damping ratio of the side ground, the equivalent damping ratio described in 4.6 and presented in Table 6 was used.

5. Seismic response analysis of Tsujun Bridge

5.1 Analysis Output

Fig. 11 shows the locations where the responses were computed. We computed the displacement response for a gravity center of 150 elements at the top of the bridge. We focused on 15 rows from row A to row O in the longitudinal direction, and 10 columns from column 1 to column 10 in the transverse direction. In total, 150 elements (15 rows \times 10 columns) were considered. The elements were named by combining the letter indicating the row and the number indicating the column. For example, the wall stone at the arch crown on the upstream side is termed "H1." The elements in the 1st and 10th columns are the wall stones, and the elements from the 2nd to the 9th columns are the soils.

In this study, we focused on the two main damage types caused to Tsujun Bridge by the Kumamoto earthquake; namely, the movement of the wall stones in the transverse direction, and the cracks in the soil that did not occur at the arch crown but rather between the arch support and the bridge deck edge. The movement of the wall stones was investigated by the displacement history in the y-direction of the top wall stones in the 1st and 10th columns. The cracks in the soil were investigated by the relative displacement history in the y-direction between the two adjacent soil elements. Thus, we obtained the relative displacement be-

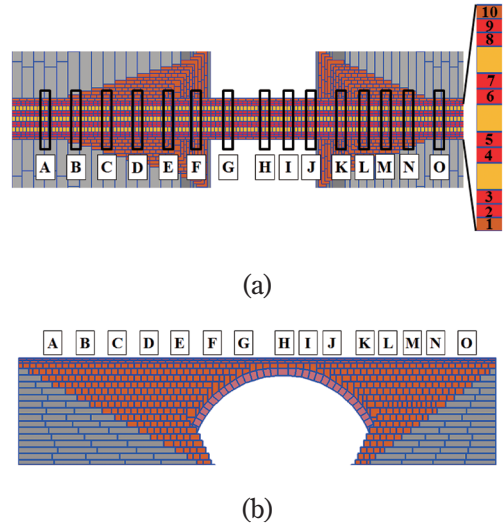


Fig. 11 Locations to output displacement responses: (a) rows and columns to output responses (view from above); (b) rows to output responses (side view from the upstream side).

Table 7 Analysis cases.

Case	Input ground motion	PGA (y-direction)
Case 1	Observed ground motion	626 gal
Case 2	Estimated ground motion 1	346 gal
Case 3	Estimated ground motion 2	207 gal

tween the 2nd and 3rd columns, 4th and 5th columns, 6th and 7th columns, and 8th and 9th columns.

5.2 Seismic response analysis

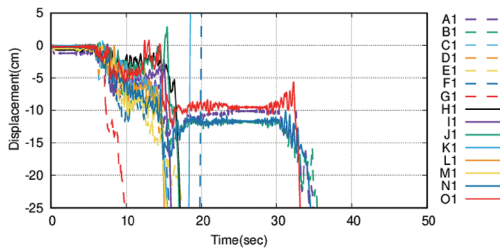
(1) Analysis cases

The analytical cases are listed in Table 7. In cases 1-3, the seismic behaviors against the three input ground motions are compared. Assuming that the ground accelerations at the base ground

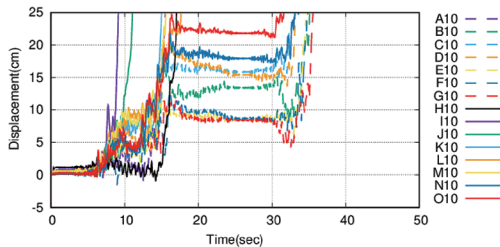
are uniform at both the left- and right-bank sides, ground accelerations as inertia forces are input to the gravity centers of all movable elements belonging to the stone bridge and the side grounds. A time interval of 2.0×10^{-4} s was employed.

(2) Results: Case 1

Fig. 12 indicates the displacement history of the top wall stones in the transverse direction (y). On the upstream side, the negative displacement indicates movement in the outward direction. On the downstream side, the positive displacement indicates movement in the outward direction. On the upstream side, almost all of the top wall stones moved outward during the foreshock, the stones in the middle from C1 to M1 fell during the foreshock, and the remaining stones (A1, B1, N1, and O1) fell during the mainshock. Similarly, all of the top wall stones fell on the downstream side.



(a)



(b)

Fig. 12 Displacement of the top wall stones in the transverse direction (case 1): (a) wall stones on the upstream side; (b) wall stones on the downstream side.

This analytical result is an overestimation because no wall stones actually fell during the Kumamoto earthquake.

Fig. 13 indicates the contour of the residual displacement of the wall stones in the transverse direction at 50 s. The positive value indicates movement in the outward direction. It should be noted that the top wall stones that had already fallen are not shown. Therefore, the movement of the soil elements is shown instead. There were many wall stones with a displacement larger than 20 cm. However, the analytical result overestimated the actual damage shown in Fig. 2(b).

Next, the relative displacements of the adjacent soil elements between the 2nd and 3rd columns, and between the 4th and 5th columns on the upstream side are shown in Fig. 14. The positive value indicates the separation between adjacent soil elements. Similar results were obtained for the soils on the downstream side. In the analytical result, cracks in the soil occurred in almost all areas, which is an overestimation of the actual situation, wherein cracks were only observed between the arch support and the bridge deck edge, as shown in Fig. 2(c). Since no soil elements fell, the relative displacement exceeding 5 cm just means that the crack width in the soil is larger than 5 cm.

In summary, the results of case 1 overestimated the actual damage. Therefore, it can be said that the observed ground motion at K-NET YABE is

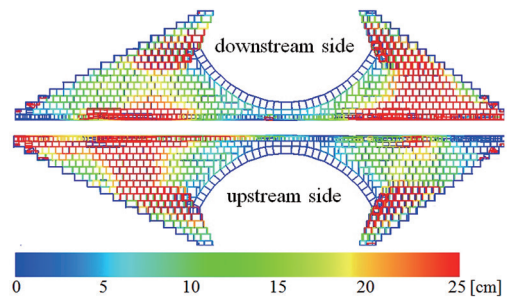
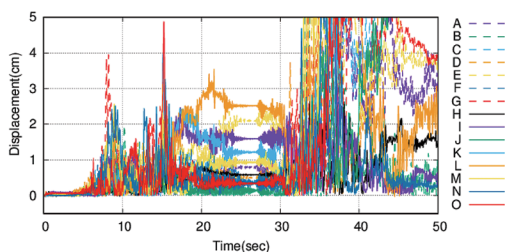
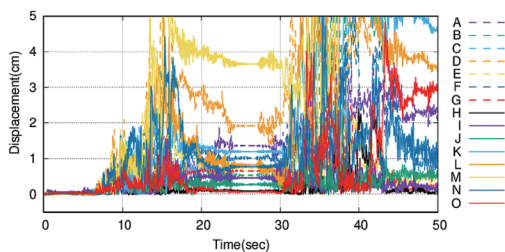


Fig. 13 Residual displacement of wall stones in the transverse direction (case 1).

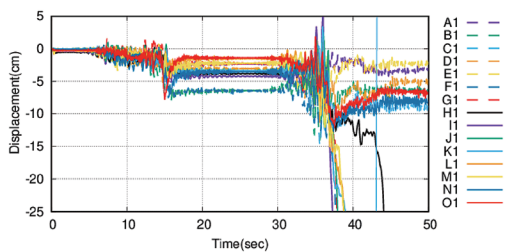


(a)

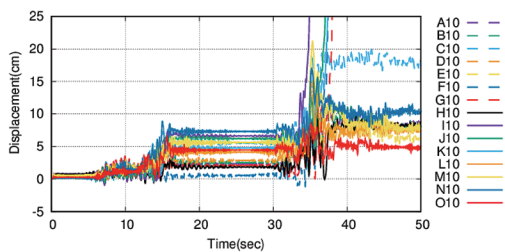


(b)

Fig. 14 Relative displacement between adjacent soil elements (case 1): (a) relative displacement between columns 2 and 3; (b) relative displacement between columns 4 and 5.



(a)



(b)

Fig. 15 Displacement of the top wall stones in the transverse direction (case 2): (a) wall stones on the upstream side; (b) wall stones on the downstream side.

different from the actual ground motion that affected Tsujun Bridge.

(3) Results: Case 2

Fig. 15 shows the displacement history of the top wall stones in the transverse direction (y). As can be seen, more than half of the stones remained. The top wall stones fell from row F to row M on the upstream side, and from rows G and I to row K on the downstream side.

Fig. 16 shows the residual displacement contour for the wall stones in the transverse direction at 50 s. The positive value indicates movement in the outward direction. Note that the top wall stones that had already fallen are not shown. Therefore, the movement of the soil elements is shown instead. In comparison to the actual displacement shown in Fig. 2(b), the result of case 2 is consid-

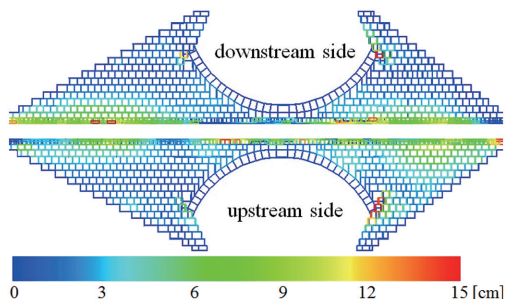
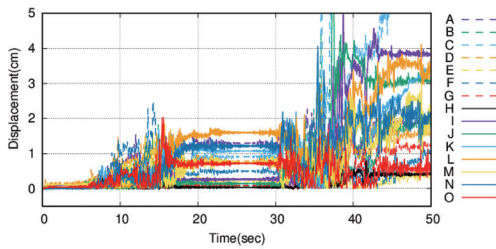


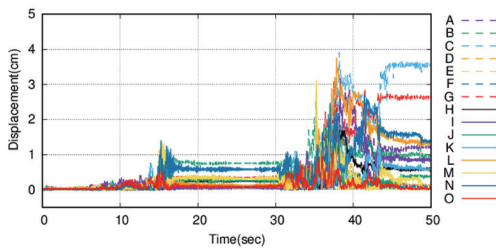
Fig. 16 Residual displacement of wall stones in the transverse direction (case 2).

ered an overestimation.

Next, the relative displacement of the adjacent soil elements between the 2nd and 3rd columns and between the 4th and 5th columns on the upstream side are shown in Fig. 17. Case 2 has a smaller relative displacement in comparison with case 1; however, cracks occurred in all rows.



(a)



(b)

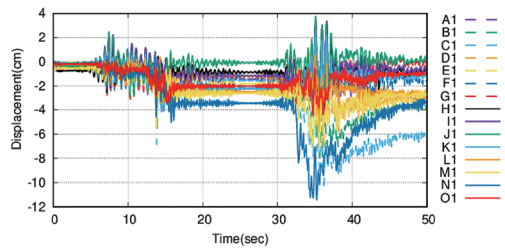
Fig. 17 Relative displacement between adjacent soil elements (case 2): (a) relative displacement between columns 2 and 3; (b) relative displacement between columns 4 and 5.

From the results presented above, it was determined that case 2 overestimated the actual damage.

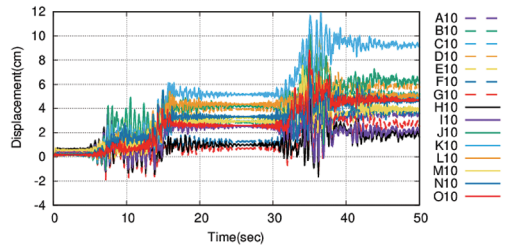
(4) Results: Case 3

Fig. 18 shows the displacement history for the top wall stones in the transverse direction (y). These stones first moved during the foreshock, and moved further during the mainshock. However, none of these wall stones fell.

Fig. 19 shows the contour of the residual displacement for the wall stones in the transverse direction at 50 s. If we focus on the top part of a bridge, displacement cannot be seen at the arch crown but rather between the arch support and the bridge deck edge. This tendency is in good agreement with the actual situation shown in Fig. 2(b). The largest displacement determined by numerical analysis was 8 cm on the upstream side and 10



(a)



(b)

Fig. 18 Displacement of top wall stones in the transverse direction (case 3): (a) wall stones on the upstream side; (b) wall stones on the downstream side.

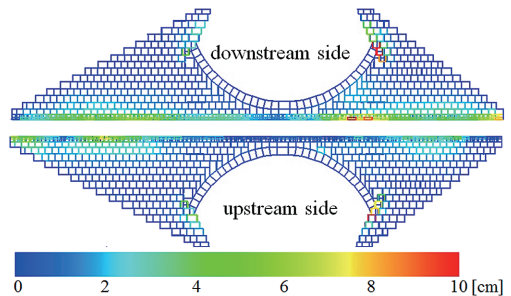


Fig. 19 Residual displacement of wall stones in the transverse direction (case 3).

cm on the downstream side. The displacement of approximately 15 cm shown in Fig. 2(b) was measured on October 20, 2016. Thus, intuition suggests that the wall stones moved not only because of the foreshock and mainshock, but also because of the earthquakes between the foreshock and the mainshock and aftershocks that occurred before October 20, 2016. Additionally, the final displac-

ment reached up to 15 cm. Therefore, the displacements of 8 cm and 10 cm were smaller than the actual displacement (approximately 15 cm) shown in Fig. 2(b).

Next, the relative displacement of the adjacent soil elements between the 2nd and 3rd columns and between the 4th and 5th columns on the upstream side is shown in Fig. 20. First, we considered the relative displacement between the 2nd and 3rd columns, which occurred on the outer side. The large relative displacement in the soils occurred from row A to row E and from row K to row O. These correspond to the location between the arch support and the bridge deck edge and are in good agreement with the actual locations of crack occurrence shown in Fig. 2(c). The residual relative displacement was approximately 1-3 cm, with the exception of row B. Then, we considered the rela-

tive displacement between the 4th and 5th columns on the interior side. The residual relative displacement was smaller than 1 cm at all locations on the inner side. This means that the relative displacement of the soil on the inner side was smaller than that of the soil on the outer side. This tendency is in good agreement with the actual situation, where in cracks occurred in the soil on the outer side, as shown in Fig. 2(c).

(5) Discussion

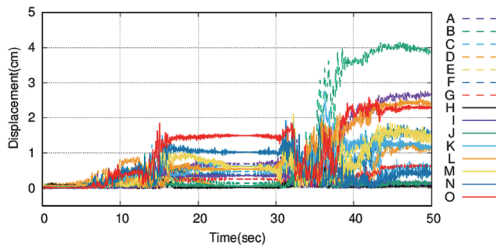
We found that the analytical results of case 3, which used estimated ground motion 2 as input, had the best agreement with the actual situation amongst all three cases. Case 1 using the observed motion as input, and case 2 using estimated ground motion 1 as input both overestimated the damage. In the next section, we will discuss why case 3 was able to simulate the actual situation.

5.3 Influence of input ground motion frequency characteristics

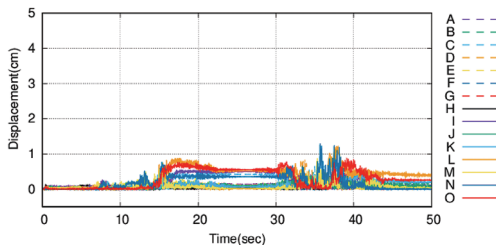
(1) Overview

Amongst cases 1-3, the analytical results of case 3 (estimated ground motion 2) are in good agreement with the actual situation, whereas case 1 (observed ground motion) and case 2 (estimated ground motion 1) overestimated the damage. Because the PGAs of case 1 and case 2 were larger than those of case 3, as shown in Table 7, intuition suggests that the damage caused by case 1 and case 2 was larger than that caused by case 3. However, the frequency characteristics of the input ground motion also affect the results.

In this section, the effect of the frequency characteristics of the input ground motion are discussed. Additional analytical cases are presented in Table 8. In case 4, the PGA of the ground motion observed in the y-direction was modified to 207 gal. In case 5, the PGA of estimated ground motion 1 in the y-direction was modified to 207 gal.



(a)



(b)

Fig. 20 Relative displacement between adjacent soil elements (case 3): (a) relative displacement between columns 2 and 3; (b) relative displacement between columns 4 and 5.

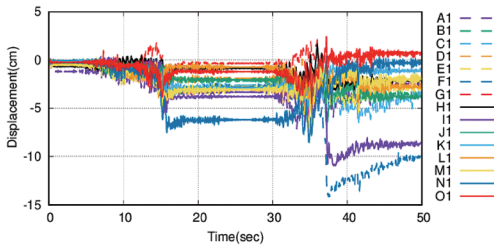
The amplitudes in the three directions were scaled down using the same scaling factor. For cases 3-5, the effects of the difference in the frequency characteristics of the input ground motion on seismic behavior are compared.

(2) Results

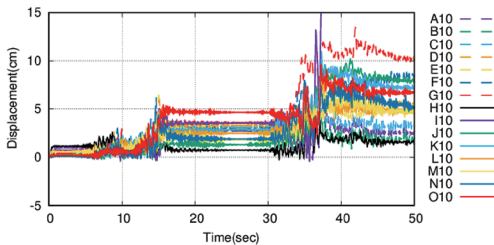
The results of case 4 are presented in Figs. 21 and 22, while those of case 5 are presented in Figs.

Table 8 Analysis cases to investigate the effect of frequency characteristics of input ground motion.

Case	Input ground motion	PGA (y-direction)
Case 3	Estimated ground motion 2	207 gal
Case 4	Amplitude-modified observed ground motion	207 gal
Case 5	Amplitude-modified estimated ground motion 1	207 gal



(a)



(b)

Fig. 21 Displacement of top wall stones in the transverse direction (case 4): (a) wall stones on the upstream side; (b) wall stones on the downstream side.

23 and 24.

Figs. 21 and 23 show the displacement of the top wall stones in the transverse direction (y). In both cases, one top wall stone fell at the arch crown (stone of row I on the downstream side for case 4; stone of row J on the upstream side for case 5).

Figs. 22 and 24 show the residual displacement

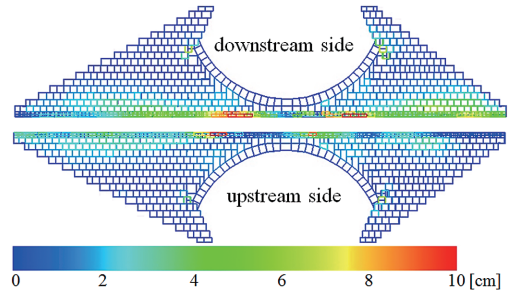
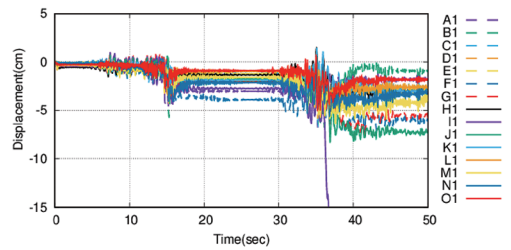
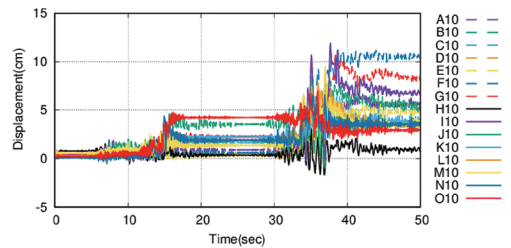


Fig. 22 Residual displacement of wall stones in the transverse direction (case 4).



(a)



(b)

Fig. 23 Displacement of top wall stones in the transverse direction (case 5): (a) wall stones on the upstream side; (b) wall stones on the downstream side.

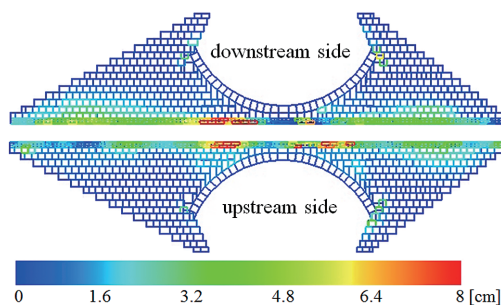


Fig. 24 Residual displacement of wall stones in the transverse direction (case 5).

ment contour for the wall stones in the y-direction after the mainshock (50 s). In both cases, the displacement of the wall stones was maximum above the arch, which is different from the actual situation. The movement of the wall stones occurred in an area wider than that in case 3 (Fig. 19).

(3) Discussion

Cases 4 and 5 had the same PGA as that of case 3 in the y-direction. However, the top wall stone above the arch fell. Moreover, the displacement of the wall stones was maximum above the arch, and could not simulate the actual damage that occurred between the arch support and the bridge deck edge. This can be explained by comparing the Fourier spectra of the microtremors observed at the bridge (Fig. 4) and the Fourier spectra of the input ground motion (Fig. 8). The input ground motion of case 3 (estimated ground motion 2) had a smaller amplitude at 3.5-9.0 Hz and a larger amplitude at approximately 10 Hz, in comparison with the other input ground motions (observed ground motion and estimated ground motion 1). This is because estimated ground motion 2 was modified by using the H/V spectral ratios shown in Fig. 6.

Microtremors were observed at point 1 and point 2 at the bridge. Point 1 is at the arch crown and corresponds to row H. Point 2 is a mid-point between the arch crown and the bridge deck edge and corresponds to row L. As shown in Fig. 4(b),

point 1 (arch crown) had a larger amplitude than point 2 (mid-point between the arch crown and the bridge deck edge) at 3.5-9.0 Hz, where the observed ground motion and estimated ground motion 1 had a larger amplitude than estimated ground motion 2. Conversely, as shown in Fig. 4(b), point 2 had a larger amplitude than point 1 at approximately 10 Hz where estimated ground motion 2 was dominant. Therefore, the displacement at the arch crown was maximum for the observed ground motion and estimated ground motion 1, while the area between the arch support and bridge deck edge increased for estimated ground motion 2. Therefore, the analytical results using estimated ground motion 2 (case 3) are in good agreement with the actual damage.

5. 4 Seismic performance investigation for Tsujun Bridge

(1) Overview

In this section, we describe the seismic performance evaluation of Tsujun Bridge using incremental dynamic analysis (IDA) (Vamvatsikos, 2002). Two seismic performances were considered. The first one is that wall stones do not fall. The second one is that the arch system does not collapse. Water leakage occurrence is also an important seismic performance, but we did not consider it since it is difficult to estimate using the current refined DEM. The seismic performance was evaluated by the PGA of the input ground motion up to which performance is guaranteed. We generated a suite of ground motions by multiplying the scale factor by the amplitudes of estimated ground motion 2, whose PGA was 207 gal. The same scale factor was used for all three directions.

To investigate the performance with no wall stones falling, we generated input ground motions whose PGA in the y-direction was 220 gal, 240 gal, 260 gal, and 280 gal.

To investigate the performance with the arch

system not collapsing, we generated input ground motions whose PGA in the y-direction was 300 gal, 400 gal, 500 gal, 600 gal, 700 gal, 800 gal, 900 gal, 1,000 gal, and 1,100 gal.

(2) Results

The wall stones did not fall under 260 gal; however, the top wall stone of C1 on the upstream side fell at 280 gal, as shown in Fig. 25. Note that 280 gal is approximately 1.35 times the PGA of estimated motion 2, which is equal to 207 gal. Therefore, the analysis result indicates that Tsujun Bridge did not have a large allowance against the falling wall stones.

The arch system of Tsujun Bridge did not collapse under 1,000 gal; however, the arch system collapsed at 1,100 gal, as shown in Fig. 26. Note that 1,100 gal is approximately 5.3 times the PGA

of estimated motion 2, which is equal to 207 gal. Therefore, the analysis result suggests that Tsujun Bridge had a large allowance against collapse of the arch system.

6. Conclusion

In this study, the damage mechanism of Tsujun Bridge during the Kumamoto earthquake was investigated by numerical analysis using the refined DEM.

First, the natural frequencies of Tsujun Bridge and the side ground were obtained by microtremor observation. Then, a numerical model was developed such that the analytical natural frequencies of the bridge and the side ground were in agreement with those obtained by microtremor observation.

Next, the H/V spectral ratios were obtained at the base ground surface of Tsujun Bridge and at K-NET YABE. Because the H/V spectral ratios were different at each site, it was found that the ground motion at Tsujun Bridge was different from the observed ground motion at K-NET YABE. Therefore, the ground motions at Tsujun Bridge were estimated using two methods. The first method was to use the bedrock ground motion at K-NET YABE as the input ground motion for Tsujun Bridge, assuming that the bridge was constructed on the bedrock. This ground motion was termed “estimated ground motion 1.” The

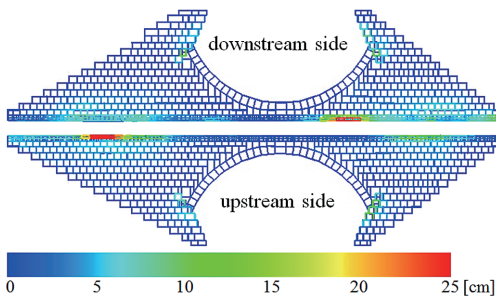


Fig. 25 Residual displacement of wall stones in the transverse direction (280 gal).

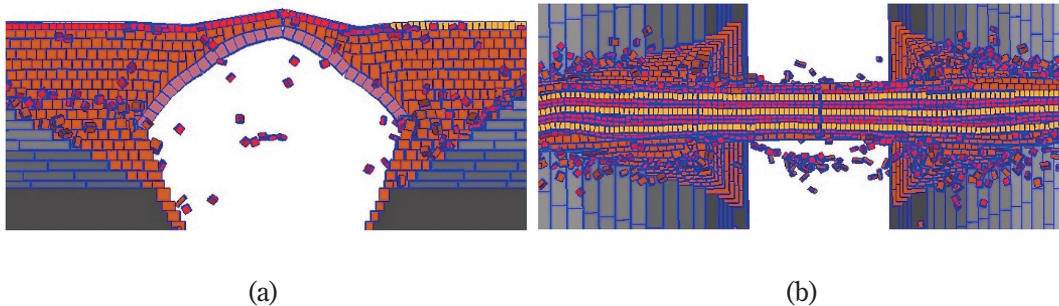


Fig. 26 Collapse of arch systems (1,100 gal): (a) front view; (b) view from above.

bedrock ground motion was estimated by multiple-reflection analysis. The second method was to modify the observed ground motion at the surface of K-NET YABE using the H/V spectral ratios at the two sites. This motion was termed “estimated ground motion 2.”

Subsequently, seismic response analysis was conducted by inputting the ground motion observed at K-NET YABE and the two estimated ground motions into the developed numerical model. The damage simulated by inputting the observed ground motion and estimated ground motion 1 overestimated the actual damage. Conversely, the damage simulated by inputting estimated ground motion 2 was in good agreement with the actual damage. In the actual situation, wall stones did not fall and the observed damage did not occur at the arch crown but rather between the arch support and the bridge deck edge. Damage was not observed between the arch support and the bridge deck edge because estimated ground motion 2 was dominant at a high frequency of approximately 10 Hz, where the vibration between the arch support and the bridge deck edge was dominant in comparison with the arch crown.

Finally, the seismic performance of Tsujun Bridge was investigated based on the critical PGAs, where the wall stones fall and the arch system collapses. Thus, it was found that the wall stones fall when the ground motion is 1.35 times as large as estimated ground motion 2. Additionally, it was found that the arch system collapses when the ground motion is approximately 5.3 times as large as estimated ground motion 2. Thus, the arch system of Tsujun Bridge was found to have had satisfactory seismic performance against the Kumamoto earthquake.

This research introduced a methodology to explain the damage occurrence mechanism of a stone bridge due to earthquakes. The proposal of a seismic reinforcement method suitable for a stone

bridge is our future work. In this study, only the effects of the foreshock and aftershock were considered, and the effects of the other aftershocks were not considered. In future works, we would like to consider the effects of other aftershocks on the failure behavior of Tsujun Bridge. Furthermore, we would like to conduct a numerical analysis based on the actual material properties and strength values evaluated by the experiment using actual materials.

Acknowledgments

We would like to express our sincere appreciation to Ms. Kyoko Otsuyama and the Board of Education, Yamato Town, Kumamoto Prefecture. Additionally, we thank Professor Kazuyuki Izuno from Ritsumeikan University for providing us with useful information. The K-NET strong-ground motion record was used in this study. Part of the present work was supported by the Japan Society for the Promotion of Science (JSPS) grant-in-aid (17H01287 and 18K04323). This support is greatly appreciated.

References

- Asai, M., Yamashita, K., Yamasaki, R., Araki, K. Estimation of static and dynamic strength of stone arch bridges by using a discrete finite element model. *Journal of Structural Engineering*, Vol. 55A, pp. 172–180, 2009.
- Architectural Institute of Japan. Design specification for special concrete structures. Tokyo, Japan, Architectural Institute of Japan, 1964.
- Cundall, P.A. Formulation of a three-dimensional distinct element model—Part I. A scheme to detect and represent contacts in system composed of many polyhedral blocks. *Int. J. Rock Mech. Min. Sci. & Geomech.*, Vol. 25(3), pp. 107–116, 1988.
- Furukawa, A., Kiyono, J., Toki, K. Proposal of a numerical simulation method for elastic, failure and collapse behaviors of structures and its application to seismic response analysis of masonry walls. *Journal of Disaster Research*, Vol. 6(1), pp.

- 51-68, 2011.
- Geospatial Information Authority of Japan, Geospatial information library. <http://maps.gsi.go.jp/>. (Accessed September 7, 2018.)
- Hagiwara, K., Izuno, K. Earthquake response to the 2016 Kumamoto earthquake and retrofitting of Tsujun bridge. *Journal of Disaster Mitigation of Cultural Heritage and Historic Cities*, Vol. 11, pp. 71-78, 2017.
- Izuno, K., Ishida, Y., Fujimoto, M., Fukagawa, R. Ambient vibration tests of Tsujun Bridge. *Journal of Japan Society of Civil Engineers, Ser. A1 (Structural Engineering & Earthquake Engineering (SE/EE))*, Vol. 73(4), pp. I_1-I_8, 2017. (In Japanese.)
- Nakamura, M., Harada, T., Wang, H., Saitoh, S. A method of estimating earthquake ground motion using microtremor H.V spectral ratio. *Journal of Japan Society of Civil Engineers, Ser. A1 (Structural Engineering & Earthquake Engineering (SE/EE))*, Vol. 65(1), pp. 65-74, 2009.
- NIED. Strong-motion seismograph networks (K-NET, KiK-net). <http://www.kyoshin.bosai.go.jp/kyoshin>. (Accessed September 7, 2018.)
- PWRI. Numerical analysis of earthquake response of ground. Report of PWRI, Vol. 1778, pp. 1-47, 1982. (In Japanese.)
- Yabe Town of Kumamoto Prefecture (Old Yamato Town). Report of repair construction work of important cultural property "Tsujun Bridge" in 1984, 1984. Accessed at Yamato Town Hall building. (In Japanese.)
- Yamato Town of Kumamoto Prefecture. Preservation and utilization plan of important cultural property "Tsujun Bridge," 2015. Accessed at Yamato Town Hall building. (In Japanese.)
- Yamato Town of Kumamoto Prefecture. Damage situation and restoration work plan of nationally designated important cultural property "Tsujun Bridge." http://www.town.kumamoto-yamato.lg.jp/life/pub/detail.aspx?c_id=46&type=top&id=613, 2016a. Accessed September 7, 2018. (In Japanese.)
- Yamato Town of Kumamoto Prefecture. Preservation and repair work of nationally designated important cultural property "Tsujun Bridge" (2). http://www.town.kumamoto-yamato.lg.jp/life/pub/Detail.aspx?c_id=46&id=945&pg=1&type=list, 2016b. Accessed September 7, 2018. (In Japanese.)
- Yamato Town of Kumamoto Prefecture. Influence of Kumamoto earthquake on April 14th and 16th in 2016 on Tsujun Bridge, 2016c. Accessed at Yamato Town Hall building. (In Japanese.)
- Yoshida, N., Kobayashi, S., Suetomi, I., Miura, K. Equivalent linear method considering frequency dependent characteristics of stiffness and damping. *Soil Dynamics and Earthquake Engineering*, Vol. 22(3), pp. 205-222, 2002.
- Vamvatsikos, D., Cornell, C.A. Incremental dynamic analysis. *Earthquake Engineering and Structural Dynamics*, Vol. 31(3), pp. 491-51, 2002.

(投稿受理：2019年3月1日
訂正稿受理：2019年7月3日)

要 旨

2016年熊本地震により、熊本県山都町に位置する重要文化財「通潤橋」には、壁石のはらみ出し、盛土の亀裂、通水管からの漏水などの被害が発生した。壁石のはらみ出しは最大15 cm程度で、その発生位置はアーチ中央部ではなくアーチ端部と橋端部の間であった。本研究では、まず、微動計測により通潤橋と周辺地盤の振動特性を明らかにした。次に、通潤橋と近傍の強震観測点での地盤の卓越周期が大きく異なることから、通潤橋地点の地震動を推定した。続いて、微動計測により明らかにした固有振動数に一致するように通潤橋の解析モデルを作成し、地震応答解析を行った。その結果、観測地震動を入力したときはアーチ中央部が破壊したのに対し、推定地震動を入力したときはアーチ端部と橋端部の間で壁石のはらみ出しが大きくなり、実被害を良好に再現することができた。